Electrochemical Synthesis of Ammonia Using Fe_3Mo_3N Catalyst and Carbonate-Oxide Composite Electrolyte

Ibrahim A. Amar, Rong Lan, Christophe T.G. Petit and Shanwen Tao[*]

Department of Chemical and Process Engineering, University of Strathclyde, Glasgow G1 1XJ, UK
[*]E-mail: shanwen.tao@strath.ac.uk

Iron molybdenum nitride catalyst (Fe_3Mo_3N) was synthesised via a temperature-programmed reduction (TPR) of the corresponding precursor by flowing pure ammonia gas. The catalyst was characterised by x-ray diffraction (XRD) and scanning electron microscopy (SEM). Ammonia was successfully synthesised for the first time from hydrogen and nitrogen at atmospheric pressure using Fe_3Mo_3N-Ag composite as cathode, Ag-Pd alloy as anode and $LiAlO_2$-carbonate composite as solid electrolyte. Ammonia formation was observed at three different temperatures 400, 425 and 450 ºC and the maximum rate of ammonia production was up to 1.88×10^{-10} mol s^{-1} cm^{-2} at 425 ºC and 0.8 V. This experiment indicates that metal nitrides can be used as ammonia synthesis catalysts in the electrochemical synthesis process.

1. INTRODUCTION

The conversion of molecular nitrogen into ammonia is a very important chemical process. Ammonia is one of the most highly produced chemicals worldwide and its global production in 2011 was 136 million metric tons [1, 2]. Additionally, ammonia finds widespread use in various industrial sectors including energy, refrigeration, transportation, fertilisers and other industries such as plastics, pharmaceuticals and explosives production, etc. The fertiliser industry is responsible for about 80 % of the global ammonia consumption [3-6].

Currently, ammonia is predominantly synthesised on a large-scale via the Haber-Bosch process which involves the reaction of gaseous nitrogen and hydrogen at high temperature and pressure [1]. Marnellos and Stoukides [7] demonstrated an alternative route to synthesise ammonia electrochemically under atmospheric pressure using solid state proton (H^+) conductors. Since then,

several proton conductors have been utilised to synthesise ammonia [8-12]. The progress of electrochemical synthesis of ammonia has recently been reviewed[13-15].

Transition metal nitrides (TMNs) have attracted considerable attention recently and have been used in a wide range of applications due to their interesting properties, including optical, magnetic, mechanical and catalytic properties [16-21]. It has been reported that metallic molybdenum has a high ability to dissociate the dinitrogen molecule (N_2) and also to form a stable nitride under ammonia synthesis conditions [20, 22]. It has been reported that molybdenum-containing nitrides such as Mo_2N, Ni_2Mo_3N, Co_3Mo_3N and Fe_3Mo_3N exhibit high catalytic activities in ammonia synthesis [23-26]. The most commonly used electrocatalysts for ammonia synthesis are precious metals such as Pd and Ag-Pd alloy [7, 8, 10]. A few reports are available in the literature on the electrolytic synthesis of ammonia using different cathode materials such as Ru- [27], perovskite- [10, 28-30] and spinel-type [31] catalysts. To the best of our knowledge, there is no report on the electrochemical synthesis of ammonia using nitride-based catalysts. Here we report the electrochemical synthesis of ammonia from H_2 and N_2 using Fe_3Mo_3N catalyst in a solid-state electrolytic cell under atmospheric pressure.

2. EXPERIMENTAL

2.1 Materials synthesis

Fe_3Mo_3N catalyst was synthesised by nitriding the corresponding precursor according to the procedure reported by Mackay et al [32]. The precursor was obtained by mixing an aqueous solution of iron nitrate ($Fe(NO_3)_3 \cdot 9H_2O$, Alfa Aesar, 98%) with an aqueous solution of ammonium heptamolybdate ($(NH_4)_6Mo_7O_{24} \cdot H_2O$, Alfa Aesar, 99%) in equimolar amounts (Fe/Mo= 1). The mixed solution was evaporated over a hot-plate under stirring until a yellow-brown solid product was obtained. The solid product was dried in the oven at 150 ºC for 2-3 *hours* then ground. The iron molybdenum nitride catalyst was synthesised via a temperature-programmed reduction (TPR) of the corresponding precursor by flowing pure ammonia gas (BOC, 100%) in a heated quartz tube. Approximately 2 g of the desired material was put in a ceramic boat and placed in the heating zone of a tube furnace. The tube furnace was programmed to heat the precursor powder in three steps as follows: the temperature was increased from room temperature to 357 ºC at a rate of 5.6 ºC min⁻¹, and then slowly from 357 to 447 ºC at 0.5 ºC min⁻¹, then to 785 ºC at 2.1 ºC min⁻¹ and then held for 5 hours at this temperature[32]. The furnace was then cooled to room temperature at a rate of 5 ºC min⁻¹ in flowing ammonia. Since the nitrided material is air sensitive, it was passivated for 1 h in flowing N_2 gas to avoid oxidation. Finally, an ultrafine black powder of Fe_3Mo_3N was obtained.

2.2 Preparation of the composite electrolyte

The ternary eutectic salt (($Li/Na/K)_2CO_3$) was prepared by solid state reaction. Lithium carbonate (Li_2CO_3, Alfa Aesar, 98%), sodium carbonate (Na_2CO_3, Aldrich, 99.5+%) and potassium carbonate (K_2CO_3, Alfa Aesar, 99%) were mixed with a molar ratio of 43.5:31.5:25 respectively. The mixture was ground and then calcined in air at 600 ºC for 1h and quenched directly to room

temperature. The composite electrolyte was made by mixing commercial lithium aluminium oxide (LiAlO$_2$, Alfa Aesar) powder with the ternary carbonate salts ((Li/Na/K)$_2$CO$_3$) at weight ratio 50:50 [31]. The mixture was ground thoroughly with an agate mortar then calcined in air at 600 $^{\circ}$C for 1 h and quenched directly to room temperature. The calcined composite electrolyte (LiAlO$_2$-carbonate) was re-ground thoroughly for subsequent use.

2.3 Materials Characterisation

X-ray diffraction (XRD) data were collected at room temperature using a Bruker-AXS (D8Advance) machine controlled by DIFFRACT plus™ software in the Bragg-Brentano reflection geometry with CuKα radiation (λ=1.5405 Å), fitted with a LynxEye^{TM} detector. XRD patterns were recorded in the 2θ range 5-85º with a step size of 0.009º and step time of 61.6 s at each step during data collection.

The microstructure of Fe$_3$Mo$_3$N catalyst was examined using a Quanta 3D FEG (FEI Company) Scanning Electron Microscope (SEM). It should be noted that, in order to obtain better image definition, the samples were coated by a thin layer of gold.

2.4 Fabrication of the single cell for ammonia synthesis

The electrolyte supported cell was fabricated by uniaxial dry-pressing the composite electrolyte powder (LiAlO$_2$-carbonate 50:50 wt%) into a 19 mm pellet under 121 MPa. The green pellet was sintered in air at 600 ºC. The composite cathode was prepared by mixing the Fe$_3$Mo$_3$N catalyst with Ag paste to increase its conductivity and adhesion to the electrolyte surface. Then the Fe$_3$Mo$_3$N-Ag composite was pasted on one side of the composite electrolyte as the cathode, with a surface area of 0.64 cm^2. Ag-Pd (Johnson Matthey, 20 wt% Pd) paste was painted on the other side as the anode. Ag wires were used as output terminals for both electrodes.

2.5 Ammonia synthesis

The fabricated single cell was placed in a self-designed double-chamber reactor. The electrolytic cell for ammonia was constructed as follows: Ag-Pd|LiAlO$_2$-carbonate|Fe$_3$Mo$_3$N-Ag. The cathode chamber was fed with oxygen-free N$_2$ (BOC Gas), whereas the anode chamber was fed with wet, highly pure H$_2$ (BOC, 99.995%). The reaction at the cathode and anode and the overall reaction have been described in a previous report[13]. The voltage was applied by a Solartron 1287A electrochemical interface controlled by software CorrWare/CorrView for automatic data collection. Constant voltage was applied and the ammonia synthesised at the cathode chamber was absorbed by 25 ml of dilute sulphuric acid (0.001 M) for 1 h. The concentration of NH$_4^+$ in the absorbed solution was analysed using Nessler's reagent (Aldrich). The produced ammonia was detected using an ammonia meter (Palintest 1000) and the rate of ammonia formation was calculated using (1:

$$r_{\text{NH}_3} = \frac{[NH_4^+] \times V}{t \times A} \qquad (1)$$

where $[NH_4^+]$ is the measured NH_4^+ ion concentration, V is the volume of the diluted H_2SO_4 used for ammonia collection, t is the absorption time and A is the effective area of the catalyst[12, 28, 31].

The average Faradaic efficiency was calculated through the total recorder charge by the Solartron 1287A during the measurements and real collected ammonia during that period of time[30].

3. RESULTS AND DISCUSSION

3.1 XRD and SEM
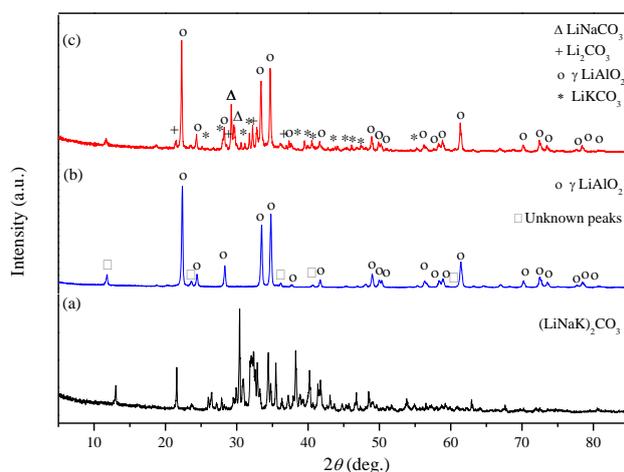
Figure 1. Powder X-ray diffraction pattern of (a) (Li/Na/K)$_2$CO$_3$; (b) LiAlO$_2$; (c) LiAlO$_2$-carbonate composite electrolyte.

Figure shows the XRD patterns of the ternary carbonate ((Li/Na/K)$_2$CO$_3$), commercial lithium aluminate (LiAlO$_2$) and LiAlO$_2$-carbonate composite electrolyte. As can be seen from Figure a, the ternary carbonates show a complicated phase composition. In the case of commercial LiAlO$_2$, the main detected peaks are indexed to γ-LiAlO$_2$ (JCPDS card no. 38-1464) with some unknown weak peaks (Figure b). The composite electrolyte is mainly composed of γ-LiAlO$_2$, Li$_2$CO$_3$ (JCPDS card no. 01-0996), LiNaCO$_3$ (JCPDS card no. 21-0954), LiKCO$_3$ (JCPDS card no. 34-1148), as shown in (Figure c). Figure represents the XRD pattern of the Fe$_3$Mo$_3$N after nitridation. As can be seen, the most intense peaks match quite well with the cubic cell of Fe$_3$Mo$_3$N (JCPDS card no. 48-1408). A small peak at 37.4º was observed, however, indicating a minor impurity, which was identified as γ-Mo$_2$N (JCPDS card no. 25-1368). γ-Mo$_2$N second phase was also found for synthesis of Co$_3$Mo$_3$N and Ni$_2$Mo$_3$N [33].
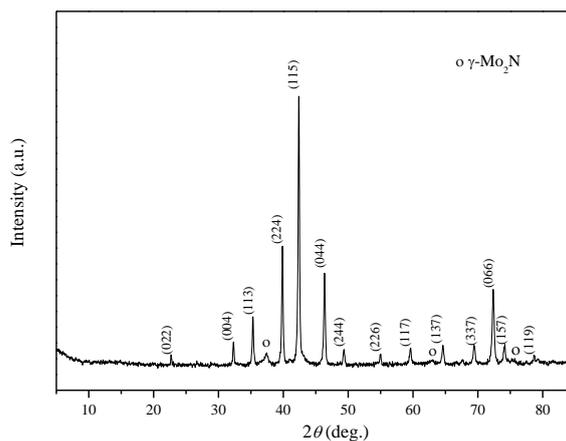
Figure 2. Powder X-ray diffraction pattern of Fe$_3$Mo$_3$N, after nitridation.
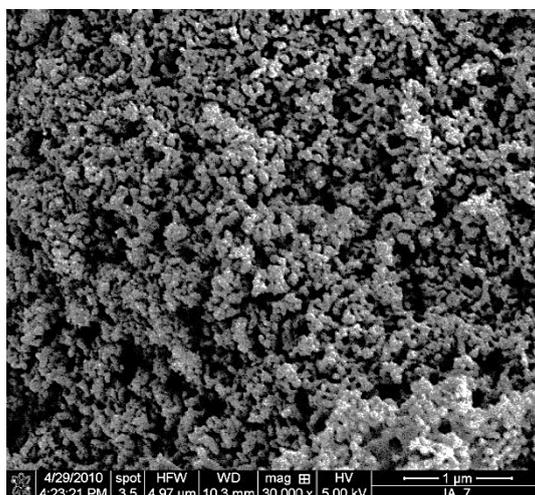
Figure 1. SEM image of synthesised Fe$_3$Mo$_3$N.

The microstructure of Fe$_3$Mo$_3$N catalyst was investigated by scanning electron microscopy (Figure 1). The morphology of Fe$_3$Mo$_3$N catalyst consists of nano-sized particles with a size range between 10 – 100 nm.

3.2 Synthesis of ammonia at different temperatures

Figure shows the electrolytic cell performance stabilities during the synthesis of ammonia at different temperatures (400-450 ℃) with an applied voltage of 0.8 V over a period of 1 h. As can be seen, the electrolytic cell demonstrated almost stable performance at all temperatures under investigation. In addition, the generated current densities increased with an increase in the cell operating temperature and reached a maximum value of 4.97 mA/cm^2 at 450 ℃. This increase in

current densities with temperature could be ascribed to the increase in the proton conductivity of the working electrolyte and decreased polarisation resistance at higher temperatures. The proton conduction of $LiAlO_2$-$(Li,Na)_2CO_3$ composite[34, 35] and $LiAlO_2$-$(Li,Na,K)_2CO_3$[31] has been reported before. It is believed that the protons are transferred through the molten carbonates or the $LiAlO_2$-carbonate interfaces.
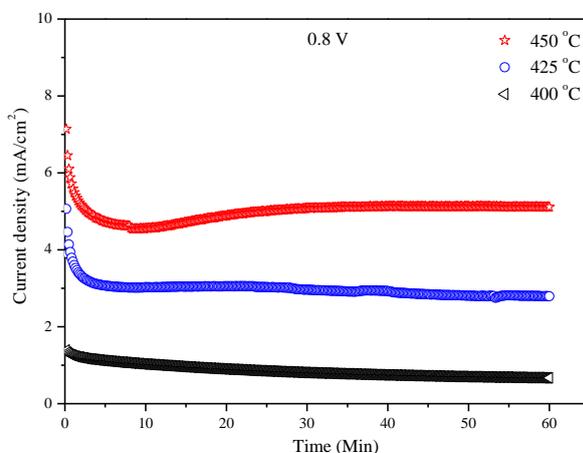

Figure 4. Electrolytic cell performance stability at 400, 425 and 450 ºC at 0.8 V: The electrolytic cell was: wet H_2, Ag-Pd|$LiALO_2$-carbonate|Fe_3Mo_3N-Ag, dry N_2.
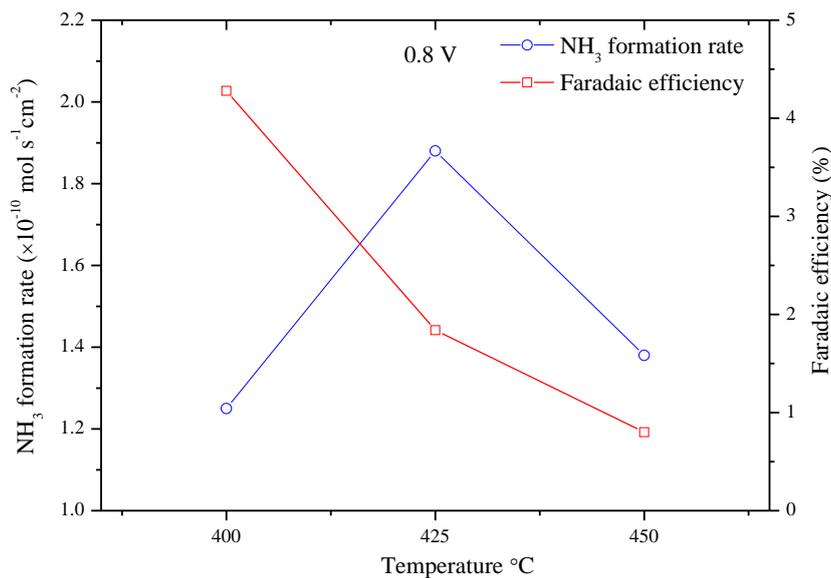
**Figure 5**. Dependence of the rate of ammonia formation on the operating temperature. The electrolytic cell was: wet H_2, Ag-Pd|$LiALO_2$-carbonate|Fe_3Mo_3N-Ag, dry N_2.

Figure 5 shows the effect of cell operating temperature on the rate of ammonia production in the electrolytic cell based on Fe_3Mo_3N-Ag composite cathode. This effect was investigated by varying the operating temperature (400-450 ºC) and keeping the cell voltage at constant value of 0.8 V over a

period of 1 h. The ammonia produced in the cathode chamber was absorbed by 25 ml of diluted sulphuric acid. When Nessler's reagent was added to the absorbed solution, its colour immediately changed to yellow. This indicates that NH_4^+ is present in the absorbed solution and thus that ammonia was successfully synthesised. As can be seen, the rate of ammonia formation increased significantly with increasing electrolytic cell operating temperature and reached a maximum value of 1.88×10^{-10} mol s^{-1} cm^{-2} at 425 °C, at which the generated current density and the corresponding Faradaic efficiency were 2.96 mA/cm^2 and 1.84% respectively. This increase in the ammonia formation rate could be ascribed to the increase of the proton conductivity of LiAlO$_2$-carbonate composite electrolyte as the cell operating temperature increased [36]. However, when the operating temperature was further increased to 450 °C, the rate of ammonia formation declined, although the electrolyte ionic conductivity increases with temperature. It could be speculated that this is due to the thermal decomposition of ammonia, which dominates at high temperature [10, 31].

Ammonia has been successfully synthesised through LiAlO$_2$-carbonate electrolyte when an oxide cathode CoFe$_2$O$_4$ was used further confirming the proton conduction of LiAlO$_2$-carbonate[31]. However, it has been reported that a small amount of Li$_3$N can dissolve in molten (Li,K,Cs)Cl molten and ammonia was formed at the anode through the reaction between H$_2$ and the transferred N^{3-} ions formed at the cathode[37, 38]. In this study, it cannot be ruled out that Fe$_3$Mo$_3$N was partially dissolved in molten carbonate then the ammonia synthesis process could be based on the N^{3-} ion route as the case for the Li$_3$N and molten (Li,K,Cs)Cl although this is unlikely because ammonia has been synthesised through an oxide cathode in the absence of nitride[31].

*3.3 Synthesis of ammonia at different applied voltages*
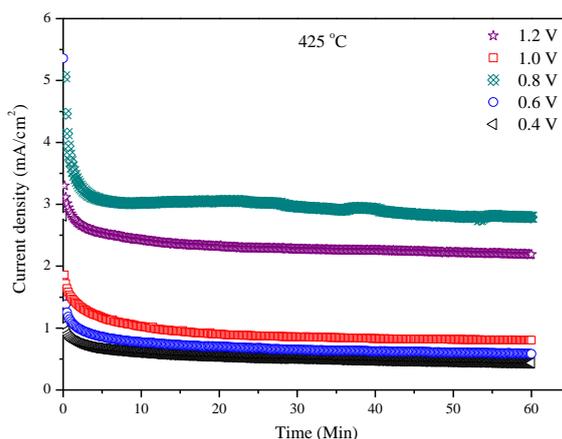
Figure 6. Electrolytic cell performance stability at 425 °C and 0.4-1.2 V: The electrolytic cell was: wet H$_2$, Ag-Pd|LiALO$_2$-carbonate|Fe$_3$Mo$_3$N-Ag, dry N$_2$.

Figure 66 shows the performance of the electrolytic cell at constant temperature (425 °C) and different applied voltages (0.4-1.2 V). After the initial decrease, the generated current densities remain almost constant at all applied voltages, indicating a stable electrochemical process. In addition, the generated current densities increased with applied voltage and the highest value of 2.96 mA/cm^2 was

obtained when the cell operated at 0.8 V. This indicates that more protons were transported through the electrolyte to the cathode. However, when the applied voltage was further increased (> 0.8 V), the generated current density decreased. Up to 0.8 V, the current increased at higher applied voltage. However, at 1.0 V, the current is lower than that at 0.8 V. The possible reason is due to the 'blocking effect' of other ions such as Li^+, Na^+, K^+ ions. At a higher applied voltage, these ions tends to move to the negative electrode (cathode). However, they cannot cross the cathode/electrode interface therefore a positively charged layer is formed on the electrolyte side of the cathode/electrolyte interface. This layer may partially block the transfer of H^+ ions, leading to lower current. On increasing the applied voltage further to 1.2 V, the electromotive force for transfer of all ions including H^+ ions increases, leading to a higher current. This phenomenon was also observed in other carbonate-oxide composite materials [39]. A similar phenomenon was also observed in the electrochemical synthesis of ammonia based on a $Li^+/H^+/NH_4^+$ conducting electrolyte [11].
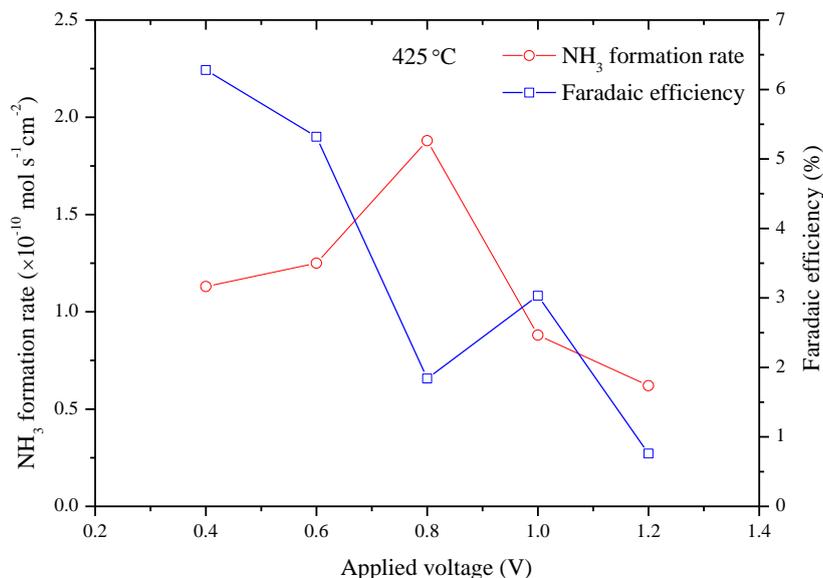

Figure 7. Dependence of the rate of ammonia formation on the applied voltage: The electrolytic cell was: wet H_2, Ag-Pd|LiALO$_2$-carbonate|Fe$_3$Mo$_3$N-Ag, dry N_2.

To investigate the effect of the applied voltage on the rate of ammonia formation, the operating temperature of the electrolytic cell was kept at a constant value and the applied voltage varied from 0.4 to 1.2 V, as shown in Figure 7. As can be seen, the rate of ammonia production increased significantly with increasing applied voltages and reached maximum values when 0.8 V was applied. Moreover, the highest rate of ammonia formation was found to be 1.88×10^{-10} mol s^{-1} cm^{-2} with an applied voltage of 0.8 V at 425 °C. However, by further increasing the applied voltage to values above 0.8 V, there was a significant decrease in the rates of ammonia formation which reached the lowest value when 1.2 V was applied. This needs further investigation. Furthermore, the low Faradaic efficiencies indicate that there is more than one reaction occurring over the cathode surface and that the competitive hydrogen

evolution reaction is the dominant one [40, 41]. At high applied voltage, hydrogen evolution became more significant[12].

4. CONCLUSION

Electrochemical synthesis of ammonia was investigated using iron molybdenum nitride catalyst (Fe_3Mo_3N) as cathode. Ammonia was synthesised from H_2 and N_2 in an electrolytic cell under atmospheric pressure at three different temperatures 400, 425 and 450 ºC respectively. The maximum rate of ammonia production was 1.88×10^{-10} mol s^{-1} cm^{-2} at 425 ºC and 0.8 V. Thus, Fe_3Mo_3N shows some catalytic properties for ammonia synthesis and further investigation is needed to improve the electrode performance to increase the ammonia formation rate.

References

1. M. Appl, Ammonia: principles and industrial practice, Wiley-VCH Weinheim, Germany, 1999.
2. US, G. Survey, Mineral Commodity Summaries, Geological Survey, 2012.
3. G.R. Maxwell, Nitrogen Products: Production and Consumption, in: Synthetic Nitrogen Products, Springer US, 2005, pp. 15-42.
4. C. Zamfirescu, I. Dincer. *J. Power Sources* 185 (2008) 459-465.
5. G.C. Miller. *J. Chem. Edu.* 58 (1981) 424.
6. H.J. Bomelburg. *Plant/Operations Progress* 1 (1982) 175-180.
7. G. Marnellos, M. Stoukides. *Science* 282 (1998) 98-100.
8. Z.J. Li, R.Q. Liu, Y.H. Xie, S. Feng, J.D. Wang. *Solid State Ionics* 176 (2005) 1063-1066.
9. Y. Guo, B. Liu, Q. Yang, C. Chen, W. Wang, G. Ma. *Electrochem. Comm.* 11 (2009) 153-156.
10. W. Wang, X. Cao, W. Gao, F. Zhang, H. Wang, G. Ma. *J. Memb. Sci.* 360 (2010) 397-403.
11. R. Lan, S.W. Tao. *RSC Advances* 3 (2013) 18016-18021.
12. R. Lan, J.T. Irvine, S.W. Tao. *Scientific Reports* 3 (2013) 1145.
13. I.A. Amar, R. Lan, C.T. Petit, S.W. Tao. *J. Solid State Electrochem.* 15 (2011) 1845-1860.
14. S. Giddey, S.P.S. Badwal, A. Kulkarni. *Inter. J. Hydrogen Energy* 38 (2013) 14576-14594.
15. I. Garagounis, V. Kyriakou, A. Skodra, E. Vasileiou, M. Stoukides. *Frontiers in Energy Research* 2 (2014) 1-10.
16. L. Roux, J. Hanus, J. Francois, M. Sigrist. *Solar Energy Materials* 7 (1982) 299-312.
17. W.R. Lambrecht, M. Miao, P. Lukashev. *J. Appl. Phys.* 97 (2005) 10D306-310D306-303.
18. P. Hones, R. Consiglio, N. Randall, F. Leacutevy. *Surf. & Coatings Tech.* 125 (2000) 179-184.
19. W. Setthapun, S.K. Bej, L.T. Thompson. *Topics in Catal.* 49 (2008) 73-80.
20. K.-i. Aika, A. Ozaki. *J. Catal.* 14 (1969) 311-321.
21. J.-G. Choi, J.R. Brenner, C.W. Colling, B.G. Demczyk, J.L. Dunning, L.T. Thompson. *Catal. Today* 15 (1992) 201-222.
22. R. Kojima, K.-i. Aika. *Appl. Catal. A: General* 215 (2001) 149-160.
23. L. Volpe, M. Boudart. *J. Phys. Chem.* 90 (1986) 4874-4877.
24. R. Kojima, K.-i. Aika. *Appl. Catal. A: General* 219 (2001) 141-147.
25. R. Kojima, K.-I. Aika. *Chem. Lett.* 29 (2000) 514-515.

26. C.J. Jacobsen. *Chem. Comm.* (2000) 1057-1058.
27. A. Skodra, M. Stoukides. *Solid State Ionics* 180 (2009) 1332-1336.
28. I.A. Amar, C.T.G. Petit, L. Zhang, R. Lan, P.J. Skabara, S.W. Tao. *Solid State Ionics* 201 (2011) 94-100.
29. R. Lan, K.A. Alkhazmi, I.A. Amar, S.W. Tao. *Appl. Catal. B: Environ.* 152–153 (2014) 212-217.
30. R. Lan, K.A. Alkhazmi, I.A. Amar, S.W. Tao. *Electrochim. Acta* 123 (2014) 582-587.
31. I.A. Amar, R. Lan, C.T.G. Petit, V. Arrighi, S.W. Tao. *Solid State Ionics* 182 (2011) 133-138.
32. D. McKay, J.S.J. Hargreaves, J.L. Rico, J.L. Rivera, X.L. Sun. *J. Solid State Chem.* 181 (2008) 325-333.
33. H.M. Wang, W. Li, M.H. Zhang. *Chem. Mater.* 17 (2005) 3262-3267.
34. R. Raza, Z. Gao, T. Singh, G. Singh, S. Li, B. Zhu. *J. Nanosci. Nanotechnol.* 11 (2011) 5402-5407.
35. S. Li, X. Wang, B. Zhu. *Electrochem. Comm.* 9 (2007) 2863-2866.
36. Z.J. Li, R.Q. Liu, J.D. Wang, Z. Xu, Y.H. Xie, B.H. Wang. *Sci. & Tech. Adv. Mater.* 8 (2007) 566-570.
37. T. Murakami, T. Nishikiori, T. Nohira, Y. Ito. *J. Amer. Chem. Soc.* 125 (2003) 334-335.
38. T. Murakami, T. Nishikiori, T. Nohira, Y. Ito. *J. Electrochem. Soc.* 152 (2005) D75-D78.
39. L. Fan, G. Zhang, M. Chen, C. Wang, J. Di, B. Zhu. *Inter. J. Electrochem. Sci.* 7 (2012) 8420-8435.
40. A. Sclafani, V. Augugliaro, M. Schiavello. *J. Electrochem. Soc.* 130 (1983) 734-736.
41. V. Kordali, G. Kyriacou, C. Lambrou. *Chem. Comm.* (2000) 1673-1674.